Atomic-scale Understanding of Catalyst Activation: Carboxylic Acid Solutions, but not the Acid Itself, Increase the Reactivity of Anatase (001) Faceted Nanocatalysts

William J. I. DeBenedetti, Erik S. Skibinski, Dapeng Jing,[†] Anqi Song,[‡] and Melissa A. Hines*

Dept. of Chemistry and Chemical Biology, Cornell University, Ithaca NY 14853 USA

Abstract

Our ability to predict nanocatalyst reactivity has been hindered by our lack of atomic-scale understanding of nanocatalyst surface structure. Do nanocatalyst surfaces adopt a bulk-terminated structure or do they reconstruct to minimize their free energy, thereby lowering their reactivity as often observed in vacuum? Similarly, do nanocatalysts processed at high temperatures maintain their low reactivity, reconstructed surfaces when used at low temperatures? Using a new technique for the preparation of anatase nanocatalysts suitable for atomic-scale imaging and surface spectroscopy, we show that solution-prepared anatase is terminated by a monolayer of fluorine, which acts as an atomic-scale oleophobic coating, preventing the accumulation of adventitious carbon. We further show that the most common TiO_2 functionalization chemistry, a carboxylic acid solution, causes the spontaneous reorganization of a reconstructed anatase nanocatalyst, leading to a five-fold increase in reactive sites. This reorganization is not observed when carboxylic acids are deposited from the gas phase, suggesting that model experiments in vacuum environments can lead to a non-equilibrium, kinetically trapped state that may not be catalytically relevant. Aqueous carboxylic acid solutions produce densely packed carboxylate monolayers with richer adsorption geometries than previously predicted. *Ab initio* simulations show that although the carboxylate termination is somewhat less effective at removing surface stress than the reconstruction, it is more effective in lowering the surface energy. This observation suggests that bulk-terminated metal-oxide nanocrystals may be common in reactive environments, even if high temperatures are used to process the nanocatalyst or if the reactant is later rinsed off. As such, the assumption of a bulk-terminated surface may be a reasonable starting point for "materials-by-design" approaches to computationally engineered nanocatalysts.

* Corresponding Author

[†] Current address: Materials Analysis and Research Laboratory, Iowa State University, Ames IA 50011 USA

[‡] Current address: Conamix, Inc., 526 Campus Road, Ithaca, NY, 14853 USA

Introduction

The atomic structure of a catalyst controls its reactivity. For example, shape-controlled synthesis, which controls the expressed facets of a nanocatalyst, can increase the reactivity[1-5] or control the specificity[6] of nanocatalysts. One natural target for this control is the prototypical nanocatalyst, anatase TiO_2, which finds use in dye-sensitized solar cells,[7–9] CO_2 photoreduction,[10] and self-cleaning or environmentally-remediating surfaces.[11,12] However, our ability to predict high-reactivity shapes has been hindered by our lack of atomic-scale understanding. Do nanocatalyst surfaces adopt a bulk-terminated structure or do they reconstruct to minimize their free energy, thereby lowering the nanocatalyst's reactivity? Similarly, do nanocatalysts activated at high temperatures maintain their low reactivity, reconstructed surfaces when used at low temperatures? Our understanding of anatase nanocatalysts has been further hindered by the poor availability of macroscopic crystals of this polymorph.

Here we use shape-controlled growth to produce highly aligned, (001)-faceted anatase nanocrystals, enabling atomic-scale imaging. We show that the most common TiO_2 functionalization chemistry,[13] a carboxylic acid solution, causes the spontaneous reorganization of a reconstructed nanocatalyst, leading to a five-fold increase in reactive sites. This reorganization is not observed when carboxylic acids adsorb from the gas phase, showing that the atomic-scale structure and reactivity of nanocatalysts in solution can be very different than that of model nanocatalysts studied in vacuum environments.

Although rutile is the most thermodynamically stable polymorph of TiO_2, anatase dominates in most commercial nanocatalysts and is an order of magnitude more photoreactive than rutile for some reactions.[14] Experiments and calculations have shown that the dominant naturally occurring anatase {101} faces are relatively unreactive. For example, H_2O and methanol do not dissociate on these surfaces.[15–17] In contrast, the bulk-terminated {001} faces, shown in Figure 1(a, b), have been predicted to be much more reactive, in part because of the large Ti–O–Ti bond angles at the surface.[15,18] However, the predicted high reactivity of this surface cannot not be tested under well controlled, ultrahigh vacuum conditions, as the (001) surface spontaneously reconstructs when the crystal is annealed, leading to the relatively unreactive (1 × 4) reconstruction shown in Figure 1(c, d).[19,20]

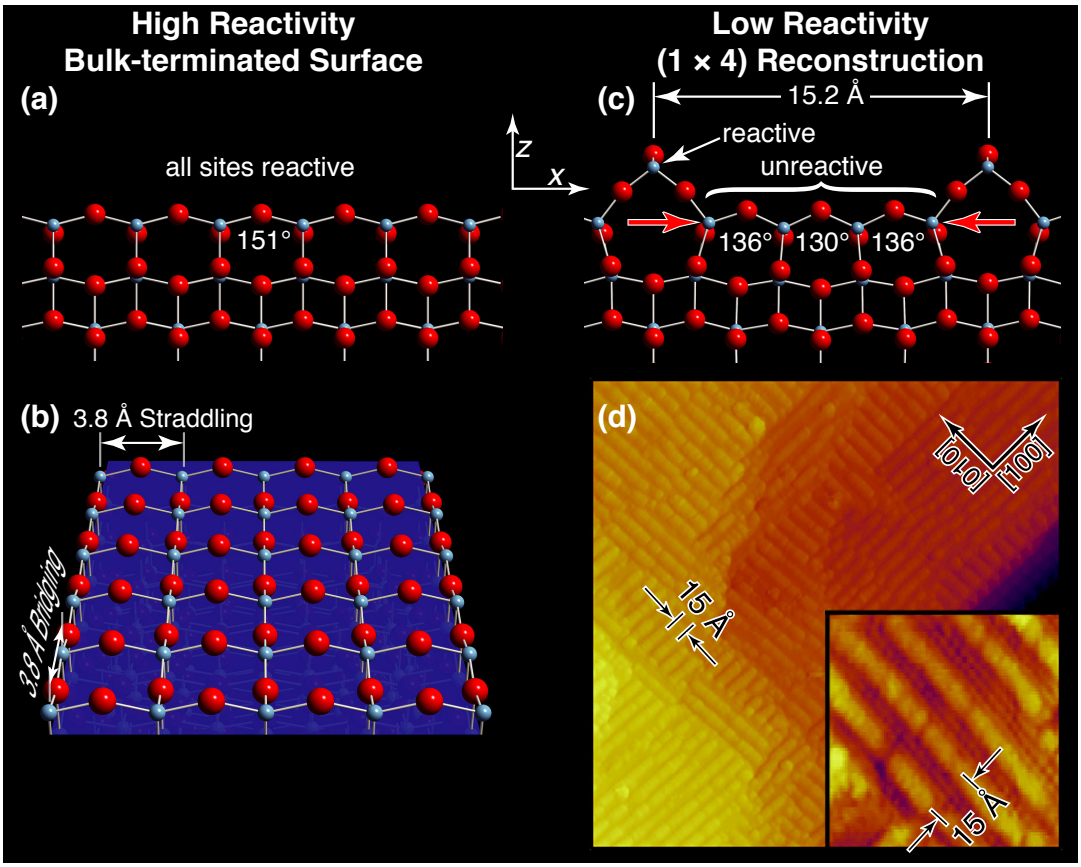

Figure 1: (a) Side and (b) top views of bulk-terminated anatase (001) . The Ti and O atoms are blue and red. (c) Side view of (1 × 4) reconstructed anatase with red arrows indicating stress relaxation. The numbers in (a, c) indicate Ti–O–Ti bond angles. The Ti–O–Ti bond angle in the added row is 148°. All structures are from DFT simulations. (d) STM image of (1 × 4) reconstructed anatase nanocrystals showing 15 Å spacing of the added rows.

Experiments in ultrahigh vacuum have confirmed that the (1 × 4) reconstruction is a low reactivity surface, with essentially inert terraces albeit reactive rows. For example, carboxylic acids do not adsorb on the reconstructed terraces, reacting only on the elevated row sites, which have a larger Ti–O–Ti bond angle than the terrace sites.[21–23] Interestingly, the terraces on the unreconstructed and reconstructed terraces have very similar bonding but different Ti–O–Ti bond angles. The structural origin of the inert terraces on the reconstructed surface has been attributed to the surface stress relaxation indicated by the red arrows in Figure 1(c).[1] Does this reconstruction also occur in catalytically relevant, reactive environments? Or does the catalyst adopt its high reactivity, bulk-terminated structure?

Shape-controlled chemical synthesis provided some indication that the bulk-terminated structure may be favorable under certain conditions. *Ab initio* calculations predicted that adsorbed fluorine would stabilize bulk-terminated {001} facets.[2] Guided by this insight, researchers used fluorine-containing solutions to

synthesize reactive anatase nanocrystals with dominant {001} faces.[2] Once synthesized, heating removed the fluorine termination, producing reactive nanocrystals; however, the small size of the nanocrystals hindered direct investigation of their surfaces. Do these crystals retain the highly reactive bulk-terminated structure after fluorine removal or do they spontaneously reconstruct to form the much less reactive surface, as suggested by experiments on TiO_2 nanowires?[24]

Here, we use shape-controlled crystal growth techniques to synthesize supported films of highly aligned nanocrystals that are well suited to investigation by a wide range of surface probes, including scanning tunneling microscopy (STM) and surface spectroscopies. We use these nanocrystals to show that carboxylic acids, one of the most commonly used functionalization chemistries for TiO_2 and other metal oxide surfaces,[13] not only stabilize anatase {001} surfaces in the bulk-terminated structure, they also *remove* a previously generated reconstruction. They do so by forming densely packed carboxylate monolayers with richer adsorption geometries than previously predicted. *Ab initio* simulations show that although the carboxylate termination is somewhat less effective at removing surface stress than the added row reconstruction, the carboxylate termination is much more effective in lowering the surface energy. This effect is primarily due to the saturation of previously unsaturated surface sites. As such, the stabilization of bulk-terminated surfaces in reactive environments may be a common feature of nanocatalysis.

Experimental and Computational

All solution-phase preparations were performed with labware that had been cleaned as described previously.[25] Ultrapure H_2O (Millipore) was used throughout, and all chemicals were used as received.

Anatase Synthesis. Supported films of anatase nanocrystals were grown by placing 0.05% Nb-doped $SrTiO_3$ (001) substrates that had been pre-annealed in air at 1000°C for 12 hr in an aqueous solution of 9 mM TiF_4, 2 mM HCl, and 0.1 M NaCl for 4 hr at 120°C in a PTFE-lined vessel. The crystallinity and alignment of the heteroepitaxial films was confirmed by x-ray diffraction performed on a Rigaku Smartlab. After growth, the F-termination could optionally be removed by sequential rinsing in 28% NH_4OH and H_2O.

Preparation of (1 × 4) Reconstructed Anatase. The samples were smoothed in ultrahigh vacuum using 3-4 cycles of sputtering with 2 μA of rastered 500 eV Ar^+ for 5 min and annealing at 720°C for 30 min.

Preparation of Benzoate-Terminated Anatase. Benzoate monolayers were prepared on initially (1 × 4) reconstructed nanocrystal films by immersion in 16 mM benzoic acid (aq, *p*H ~ 3.0) at 100°C for 2 min.

Scanning tunneling microscopy. STM analysis was performed at room temperature in ultrahigh vacuum using a W tip and a Omicron variable-temperature STM. The tunneling conditions were 90-100 pA at 2.10-2.20 V.

X-ray photoemission spectroscopy. X-ray photoelectron spectroscopy (XPS) was performed using an unmonochromated Mg Kα source; the photoelectrons were collected at 70° from the surface normal. A Tougaard baseline was subtracted from each spectrum, and a small energy correction (~0.05 eV) was applied to reported spectra using published energies. The Ti 2*p* and O 1*s* spectra were normalized to the same maximum intensity. The C 1*s* and F 1*s* spectra were normalized to the integrated intensities of the corresponding (unnormalized) Ti 2*p* spectra.

Infrared spectroscopy. Anatase films for infrared spectroscopy were grown on 10 mm × 10 mm × 0.5 mm undoped $SrTiO_3$ substrates that had been beveled at 45° along opposite edges. Films for infrared investigation were heated to 350°C for 30 min in air to remove trapped H_2O. Infrared spectra were collected in a dry-air-purged Fourier transform infrared spectrometer (Nicolet 670) with a mercury-cadmium-telluride detector and a ZnSe wire grid polarizer (Molectron) in either the glancing incidence reflection (80° incidence, ≤ 2000 cm^{-1}) or multiple-internal-reflection (MIR, > 2000 cm^{-1}) geometries. Spectra taken in the MIR geometry were referenced to a sample that had been heated to 350°C in air for 30 min. Spectra taken in the glancing incidence geometry were referenced to a phenylphosphinate-terminated sample that was prepared by immersing a clean sample in 13 mM aq. phenylphosphinic acid (Sigma, >99%) using previously published methods.[26]

***Ab-initio* Simulations.** Density functional theory (DFT) calculations were performed within the generalized gradient approximation[27] (GGA) with the Perdew, Burke, and Ernzerhof (PBE) exchange-correlation functional[28] which was corrected for long-range dispersion interactions using the zero-damping DFT-D3 method[29] as implemented in the Vienna *ab initio* simulation package (VASP).[30,31] Electron-ion interactions were described using the projector augmented wave (PAW) method.[32] The models used 2 × 1, 1 × 2, and larger periodically repeating 17-Å-thick anatase slabs separated by a 12.5 Å vacuum space, where the first and second integers refer to the number of repeat units in the [100] and [010] directions, respectively. During geometrical optimization, the positions of the atoms in the bottommost anatase layer were held fixed in their bulk positions. Brillouin-zone integration was performed using Gaussian smearing. Electronic states were expanded in plane waves with a kinetic energy cutoff of 400 eV (520 eV for stress calculations) and a 7 × 5 × 1 Monkhorst-Pack grid of *k* points for the 1 × 2 supercell. Larger supercells used proportionally fewer *k* points. STM images were modeled within the Tersoff-Hamann approximation[33] as isosurfaces of constant local density of states in an energy band from 0.66 eV below the highest occupied band to the Fermi energy. Additional description and structures are in the Supplementary Information.

Results

F-terminated nanocrystals are atomically clean and oleophobic: We synthesized supported films of anatase nanocatalysts expressing predominantly {001} facets from aqueous TiF_4 solutions on atomically

flat $SrTiO_3$ (001) surfaces as shown by the SEM image in Figure 2. The $SrTiO_3$ (001) surface is a near lattice match (3.2% strain) to the anatase (001) face, and the nanocrystals deposit heteroepitaxially, as shown by x-ray diffraction analysis (Supplementary Info).

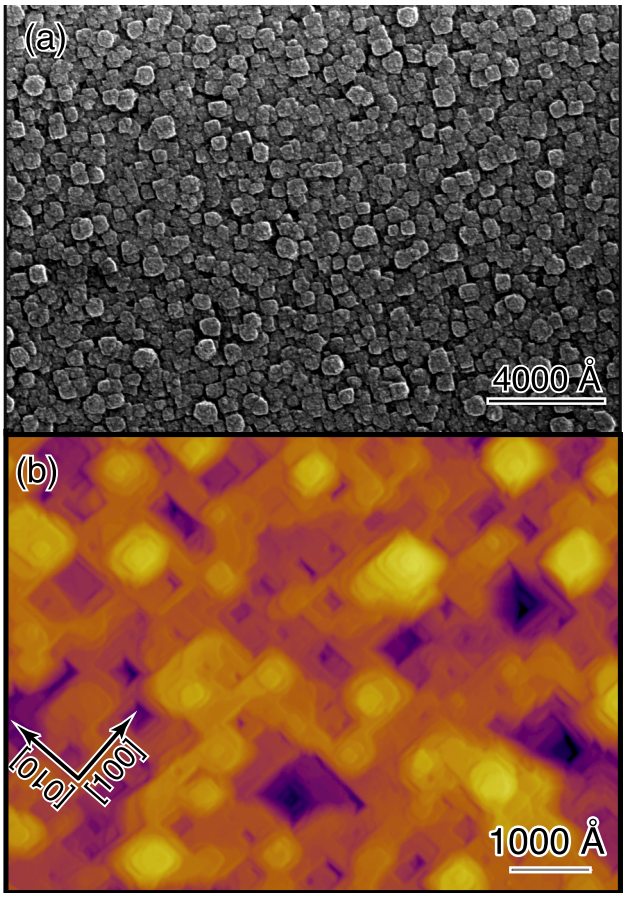

Figure 2: Highly aligned supported anatase nanocatalysts expressing predominantly {001} facets as imaged in (a) SEM as grown and (b) STM after sputter-annealing.

As seen in Figure 3, x-ray photoemission spectroscopy (XPS) showed that the as-synthesized crystals were terminated with a monolayer of F as predicted by *ab initio* simulations,[2,34] with some bulk F incorporation. High resolution scans of the Ti 2*p* region were dominated by the Ti $2p_{1/2}$ and $2p_{3/2}$ transitions characteristic of Ti^{4+} in bulk TiO_2. After the nanocrystals were sputter-annealed, a small shoulder characteristic of Ti^{3+} defects was observed. High resolution scans of the O 1*s* region were dominated by the 530.3 eV transition characteristic of O in bulk TiO_2. A broad transition at ~533 eV was observed in the as-deposited films, which was attributed to OH and H_2O trapped in the film by comparison with published spectra of H_2O on rutile (110)[35] and anatase (001).[36] High resolution scans of the F 1*s* region showed evidence of F incorporation into the films as well as F termination of the as-grown crystals. Quantification of the F 1*s* spectra (Supplementary Info) showed the nanocrystals were terminated by 75 ± 25% of a monolayer of F.

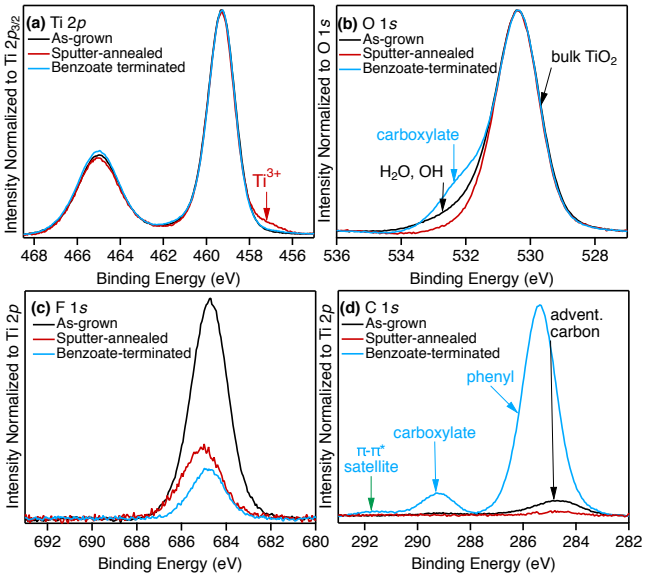

Figure 3: X-ray photoemission spectra of anatase nanocatalyst (black) as grown, (red) after sputter-annealing, and (blue) after termination with a benzoate monolayer. The transition assignments are shown in the same colors.

In spite of being synthesized in solution and handled in air, the nanocrystals were very clean with only trace adventitious carbon as seen in Figure 3(d). In contrast, a relatively thick adventitious C film was observed on shape-controlled anatase nanoparticles[2] and nanorods.[24] High resolution scans of the C 1*s* region showed a very small amount of adventitious carbon in the as-deposited films which disappeared after sputter-annealing. After benzoate deposition, transitions attributed to carboxylate C at 289.2 eV and phenyl C at 285.4 eV were observed and assigned in analogy to published spectra of benzoate on rutile (110).[25,37] Using the carboxylate transition as an absolute standard, the adventitious C on the as-synthesized crystals was measured to be less than 14% of a monolayer!

When the fluorine termination was removed either chemically or by sputtering, the nanocrystals accumulated adventitious carbon in air, which showed that the fluorine termination passivates the surface and acts as an atomic-scale, oleophobic coating. When the fluorine monolayer was removed with a NH_4OH rinse, a characteristic carboxylate transition at 289.8 eV appeared as seen in Figure 4, which we assigned to bicarbonate formed from the catalytic reaction of CO_2 and H_2O in analogy to rutile (110).[38]

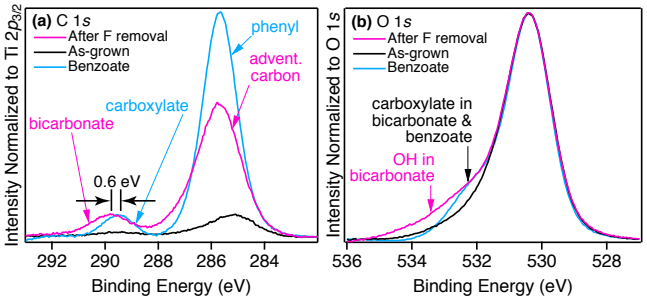

Figure 4: X-ray photoemission spectra of anatase nanocatalyst (magenta) after removal of F monolayer with NH_4OH showing dramatic increase in adventitious C. XPS spectra of (black) as-grown and (blue) benzoate-terminated nanocrystals are shown for comparison.

Carboxylic acid solution removes surface reconstruction: Nanocrystal films with (1 × 4) reconstructed surfaces were prepared by mild sputtering and annealing to 720°C in ultrahigh vacuum, which also induced sufficient conductivity for STM. As shown by Figure 1(d), the (1 × 4) reconstructed surface was characterized by 2-Å-high elevated rows separated by 15 Å. The added rows were parallel to one another on a given atomic plane; however, the row direction rotated by 90° on successive atomic planes, running parallel to either the [100] or [010] direction.

In stark contrast to experiments in ultrahigh vacuum,[21–23] a carboxylic acid (here, benzoic acid) deposited from an aqueous solution not only adsorbed on the terraces, it completely removed the (1 × 4) reconstruction, as shown by Figure 5(a). Using the procedure developed for rutile TiO_2,[25] benzoate monolayers were prepared on initially (1 × 4) reconstructed nanocrystal films by immersion in 16 mM benzoic acid at 100°C for 2 min. This produced dense, close-packed monolayers of benzoate as seen in STM in Figure 5(a). No evidence of the original (1 × 4) reconstruction or its 15 Å periodicity was observed. Instead, the images displayed parallel rows of molecules with a 4 Å spacing within each row and an 8 Å spacing between individual rows. In contrast to the (1 × 4) reconstructed surface, individual terraces displayed rows running parallel to both the [100] and [010] directions. In other words, the STM images displayed regions of (1 × 2) and (2 × 1) symmetry on the same atomic plane.

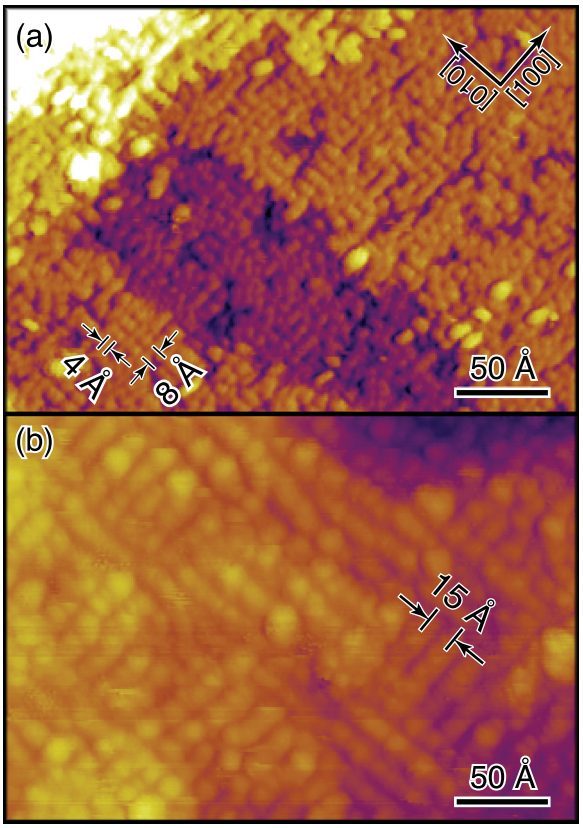

Figure 5: (a) STM image of initially (1 × 4) reconstructed anatase nanocrystals after immersion in 16 mM benzoic acid (aq.). The 15 Å spacing of the reconstruction is no longer observed. Instead, the adsorbed benzoate molecules form regions of (1 × 2) and (2 × 1) symmetry. (b) STM image of reconstructed nanocrystals after sequential immersions in pure H_2O, 0.3 M HF, and H_2O showing retention of the (1 × 4) reconstruction.

Figure 5(a) shows that carboxylic acid solutions induce a spontaneous rearrangement of anatase (001) surfaces, leading to a more reactive structure. When the (1 × 4) reconstruction is exposed to a carboxylic acid in ultrahigh vacuum (UHV), only the row-top sites, which comprise 20% of all surface Ti sites, are reactive.[21–23] In contrast, aqueous benzoic acid removed the (1 × 4) reconstruction, rendering all of the surface Ti atoms reactive.

The (1 × 4) reconstruction is not removed by all aqueous solutions or even by all acidic solutions, at least on the time scale of minutes. For example, Figure 5(b) shows a (1 × 4) reconstructed surface after sequential 30 s immersions in pure H_2O, 0.3 M HF, and copious H_2O rinsing. After this, the (1 × 4) reconstruction remained.

Infrared spectroscopy confirms benzoate formation: The infrared spectra of benzoate-terminated anatase (001) nanocrystals were strikingly similar to spectra of benzoate-terminated rutile (110),[25,26,39] a

system in which benzoate is known to bond in a vertical, bridged bidentate geometry. The observed modes are summarized in Table 1 and discussed in the following.

	Energy (cm^{-1})		Anatase
	Anatase (001)	**Rutile (110)**	**Polarization**
C–H Str.	3092	3092	–
C–H Str.	–	3070	–
C–H Str.	3062	3062	–
C–H Str.	–	3056	–
C–H Str.	3034	3034	–
ν_{asym}(OCO)	1527	1489	in plane
ν_{sym}(OCO)	1435	1427	*z*

Table 1: Summary of benzoate vibrational modes observed on benzoate-terminated anatase (001) nanocrystals and benzoate-terminated rutile (110). The rutile data are from Refs. 25, 26, and 39.

Infrared spectra of benzoate-terminated anatase (001) obtained in the multiple-internal-reflectance (MIR) geometry, shown in black in Figure 6, displayed modes at 3034 cm^{-1}, 3062 cm^{-1}, and 3092 cm^{-1}, which were assigned to aromatic C–H stretch modes in analogy with previously observed modes on benzoate-terminated rutile (110), which are shown in red. The anatase (001) surface has macroscopically C_4 symmetry, whereas the rutile (110) surface has C_2 symmetry. As a result, all in-plane-polarized spectra are identical on anatase (001), whereas there are two distinct in-plane polarizations (*i.e., x* and *y*) on rutile (110). Because of this higher symmetry and the multilayer $TiO_2/SrTiO_3/TiO_2$ substrate, we were unable to use the Cartesian transformation techniques[39] that enabled the resolution of two additional C–H stretch modes at 3056 cm^{-1} and 3070 cm^{-1} on benzoate-terminated rutile (110). Importantly, no aliphatic C–H stretch modes, which have stretching vibrations < 3000 cm^{-1}, were observed.

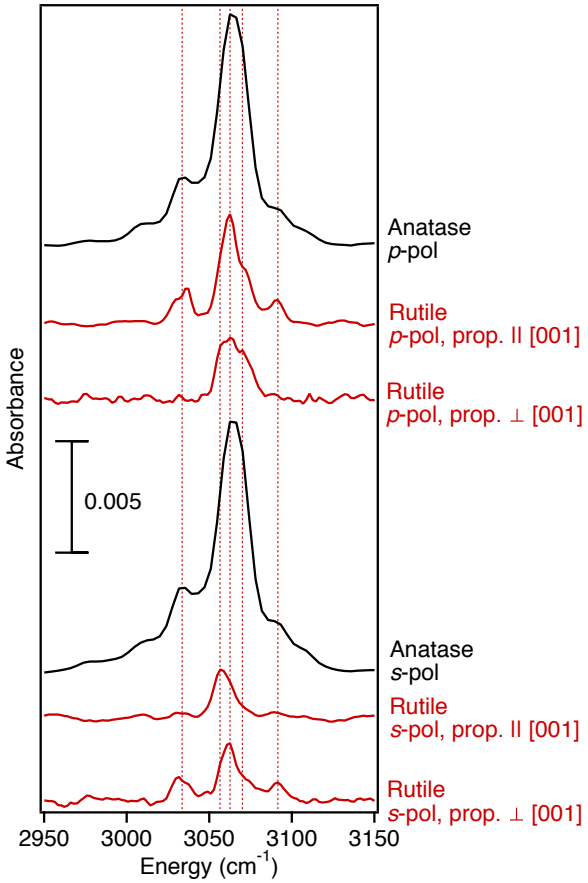

Figure 6: Infrared spectra of (black) benzoate-terminated anatase (001) nanocrystals and (red) benzoate-terminated rutile (110) referenced to thermally and chemically cleaned samples, respectively. The dotted red lines at 3034 cm^{-1}, 3056 cm^{-1}, 3062 cm^{-1}, 3070 cm^{-1}, and 3092 cm^{-1} represent transitions previously identified on rutile (110).

The absorbances of spectra taken in the MIR geometry on anatase (001) nanocrystals were significantly and consistently larger than the absorbances of comparable modes on rutile (110), as seen in Figure 6. No similar enhancements were observed in XPS spectra or in infrared spectra taken in reflectance. Therefore, we hypothesize that these enhancements are an optical effect caused by the multilayer $TiO_2/SrTiO_3/TiO_2$ structure; however, we have yet to perform the necessary modeling to test this hypothesis.

Infrared spectra obtained in the reflectance geometry, shown in black in Figure 7, confirmed that the OCO moiety in benzoate is bound in a nominally vertical configuration, consistent with the bridged bidentate geometries suggested by the STM images and DFT calculations (*vide infra*). The modes at 1435 cm^{-1} and 1527 cm^{-1} were assigned to the symmetric and asymmetric OCO stretch vibrations on anatase (001), respectively, in analogy with previously observed modes on rutile (110) which are shown in black. We attribute the somewhat different splittings between these modes on anatase and rutile to the somewhat

different bonding geometry, as the Ti–Ti distances on anatase (001) and rutile (110) are 3.8 Å and 3.54 Å, respectively. Polarization analysis in the reflectance geometry is complicated by the fact that, depending on the incidence angle of the radiation and the polarization of the mode, infrared absorption by the monolayer can either *increase or decrease* the amount of reflected light. As discussed in detail in Ref. 26, the polarization dependence of the symmetric and asymmetric OCO stretch vibrations observed on benzoate-terminated rutile (110) is indicative of modes oriented perpendicular and parallel to the surface, respectively. The same polarization dependence was observed on benzoate-terminated anatase (001), indicating that this OCO moiety is also bound in a nominally vertical configuration.

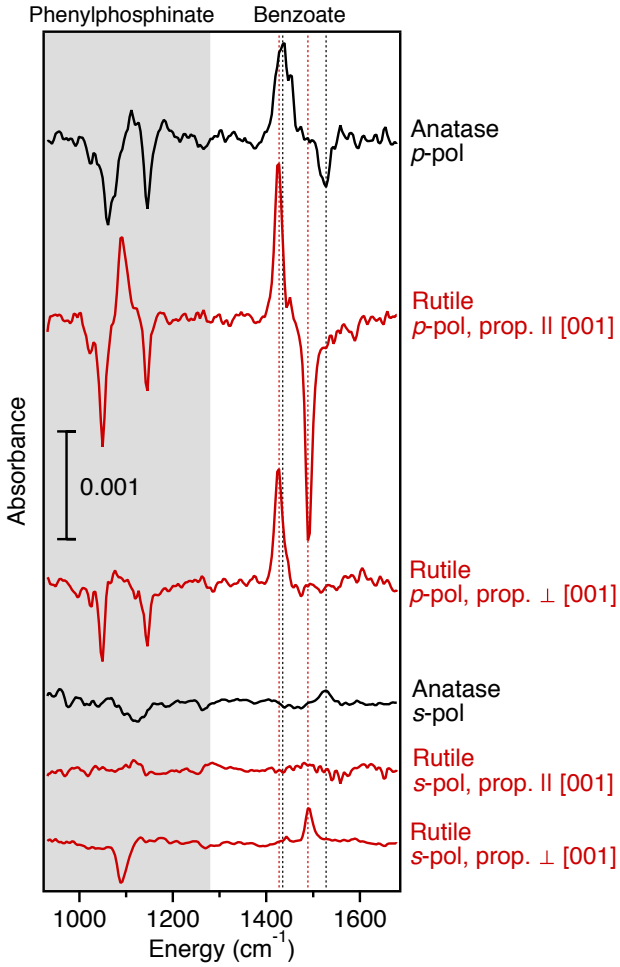

Figure 7: Reflectance infrared spectra of (black) benzoate-terminated anatase (001) nanocrystals and (red) benzoate-terminated rutile (110) referenced to the corresponding phenylphosphinate-terminated samples. The dotted black lines at 1435 cm^{-1} and 1527 cm^{-1} indicate the OCO symmetric and asymmetric symmetric vibrations, respectively, on anatase whereas the dotted red lies at 1427 cm^{-1} and 1489 cm^{-1} indicate the corresponding vibrations on rutile (110). The modes in the gray-shaded region are phenylphosphinate modes as discussed in Ref. 26.

Surface energy drives lifting of the reconstruction: The structure of the adsorbed benzoate monolayer was modeled using density functional theory (DFT). Two nearly isoenergetic bridging bidentate isomers were identified as shown in Figure 8, the "bridging" and "straddling" configurations. In the chemically intuitive "bridging" structure, benzoate binds to two undersaturated Ti atoms that are connected by a saturated O atom, while the liberated proton binds to an undersaturated O atom and H-bonds to an adjacent undersaturated O atom. In the less intuitive "straddling" structure, benzoate binds to two undersaturated Ti atoms and straddles an undersaturated O atom, which is significantly displaced into the surface as indicated by the red arrow in Figure 8. The H atom binds to the remaining undersaturated O atom. Simulated STM images of the two isomers, also shown in Figure 8, agreed with experiment. Consistent with previous studies,[40] structures in which benzoate binds to a single Ti atom were significantly less stable (Supporting Information).

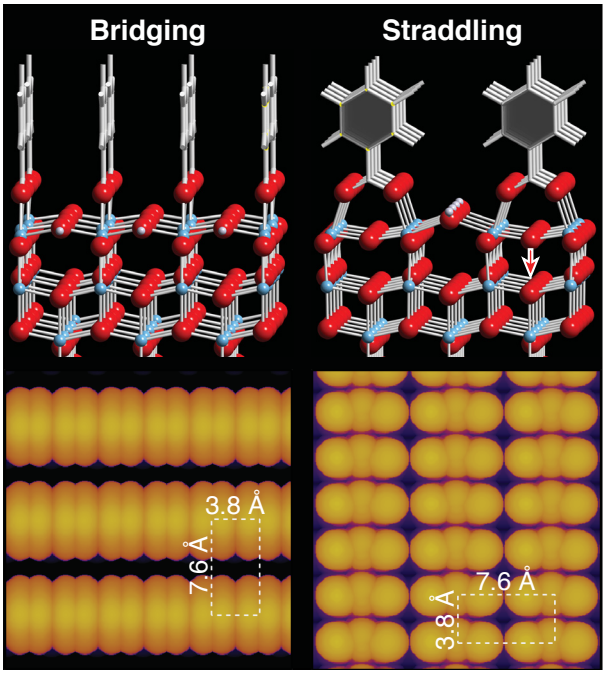

Figure 8: (Top) Structures of two nearly isoenergetic bridging bidentate isomers, the "bridging" and "straddling" isomers, identified from DFT simulations. The red arrow indicates displacement of the surface O atom. The Ti, O, and H atoms are blue, red, and white, respectively. (Bottom) Simulated STM images of the two isomers, showing the same (1 × 2) and (2 × 1) symmetries observed experimentally.

The formation of the (1 × 4) reconstructed surface has been rationalized in terms of surface stress reduction;[20] however, the lifting of the (1 × 4) reconstruction by benzoate cannot be rationalized in similar terms. DFT calculations of surface stress, reported in Table 2, show that although the benzoate-terminated

surface has a significantly lower stress than the clean, bulk-terminated surface, it is more stressed than the bare (1 × 4) reconstructed surface.

System		Surface Energy	Surface Stress
Bare	Bulk terminated	1.30	5.42
	(1 × 4) reconstruction	0.88	1.80
Benzoate	(1 × 4) recon. (UHV)	0.62	2.39
	Straddling (obs.)	0.20	2.45
	Bridging (obs.)	0.18	2.17

Table 2: Calculated surface energies and stresses (g_{xx}) in J m^{-2} for a variety of bare and benzoate-terminated anatase structures. Although the bare (1 × 4) reconstructed surface has minimum surface stress, the experimentally observed straddling and bridging benzoate isomers have minimum surface energy. The carboxylate-terminated (1 × 4) reconstructed surface is only observed in ultrahigh vacuum.[23,24]

The stabilization of the bulk-terminated surface by benzoate is better rationalized in terms of the surface energy, as DFT simulations showed that the benzoate-terminated, unreconstructed surface had the lowest surface energy (Table 2). Simply put, the surface energy stabilization from terminating all of the surface Ti atoms in the experimentally observed structure more than compensates for the higher stress of the unreconstructed surface.

To test whether any of these effects are due to the nature of the carboxylic acid, all simulations were repeated using the smallest carboxylic acid, formic acid. Similar structures, binding energies, stresses, and surface energies were observed (Supporting Information). From this we concluded that the energetic effects are primarily due to interactions of the carboxylate group and are minimally influenced by the organic "tail." Thus, we expect that all carboxylic acid solutions should have similar effects, unless steric bulk prevents the formation of a complete monolayer (*e.g.,* large dye molecules[13]).

Discussion

The DFT calculations summarized in Table 2 imply that carboxylic acid deposition in vacuum leads to a non-equilibrium, kinetically trapped state, as the carboxylate-terminated (1 × 4) reconstructed surface observed in ultrahigh vacuum has a significantly higher surface energy than the carboxylate-terminated unreconstructed surface. Even at the low reactant concentrations used in this experiment, solution environments are kinetically advantaged over ultrahigh vacuum reactions because of the much higher reactant fluxes to the surface as well as the greatly reduced activation barriers to desorption in aqueous

environments. Both effects are likely important. We hypothesize that the principal difference between the two environments is the ease of forming soluble carboxylate-terminated titanium oxo clusters in solution. (For example, see Ref. 41.) Indeed, the ragged step edges and multilayer vacancy islands (*i.e.,* pits) observed in Figure 5(a) suggest that the (1 × 4) reconstruction is removed through an etching process. Irrespective of mechanism, these experiments illustrate that the atomic-scale structure and reactivity of nanocatalysts in solution may be very different than suggested by experiments in ultrahigh vacuum.

The stability of the (1 × 4) reconstruction in HF solutions was unexpected, as previous DFT calculations of surface energies had predicted the formation of unreconstructed fluorine-terminated anatase (001) surfaces in aqueous HF.[42] Chemical analysis of the HF-treated, (1 × 4) reconstructed surfaces showed no detectable fluorination, and rutile (110) was similarly stable to fluorination even after immersion in 49% HF. Instead, XPS spectra of both chemically cleaned and HF-treated surfaces showed a pronounced carbonate transition in the C 1*s* region, which strongly resembled the transitions observed on air- and solution-treated rutile (110).[38] We concluded that clean anatase (001) catalyzes the same reaction of ambient CO_2 and H_2O as rutile TiO_2 (110), forming a stable, tightly bound bicarbonate (HCO_3) termination.[38] Thus, the stability of the (1 × 4) reconstruction in HF solutions is likely due to the bicarbonate layer, which was not considered in the DFT calculations.[42] Like all carboxylates, the bicarbonate layer is stabilized energetically by its strong bonds to the surface as well as entropically by its bidentate bonding.

The bulk-terminated surface structure is expected to be stable under typical reaction conditions (*e.g.,* ≤ 300°C for solution processing), as formation of the (1 × 4) reconstruction on the nanocrystals in ultrahigh vacuum required significant thermal activation (≥550°C). Thus, even though benzoic acid does not permanently passivate the anatase (001) surface and is readily rinsed away with H_2O, the high reactivity of the bulk-terminated surface structure should persist and be stable under typical catalytic conditions. Consistent with this, we have never observed regeneration of the (1 × 4) reconstruction during solution processing.

The observation that one of the most commonly used functionalization chemistries, aqueous carboxylic acid, removes a reconstruction from the prototypical metal oxide nanocatalyst, anatase, suggests that bulk-terminated nanocrystals may be common in reactive solution-processing environments, even if high temperatures are used to synthesize or calcine the nanocatalyst. This observation also suggests that the assumption of a bulk-terminated surface may be a reasonable starting point for "materials-by-design" approaches to engineered nanocatalysts which use computational methods to guide the selection of materials parameters (*e.g.*, doping, defects, compound oxides).

Conclusions

The most common TiO_2 functionalization chemistry, a carboxylic acid solution, causes the spontaneous reorganization of a reconstructed anatase nanocatalyst, leading to a five-fold increase in reactive sites and the formation of a bulk-terminated surface structure. Even though the carboxylate-termination is readily rinsed off in aqueous solutions, the bulk-terminated structure remains, as formation of the (1 × 4) reconstruction requires thermal activation (≥550°C) inaccessible under typical solution processing conditions. This finding suggests that bulk-terminated metal-oxide nanocrystals may be common in reactive solution-processing environments, even if high temperatures are used to synthesize or calcine the nanocatalyst. This reorganization is not observed when carboxylic acids adsorb from the gas phase, showing that the atomic-scale structure and reactivity of metal-oxide nanocatalysts in solution can be very different from that of model nanocatalysts studied in vacuum environments.

Anatase nanocrystals synthesized in fluorine-containing solutions are terminated by a monolayer of fluorine, which acts as an atomic-scale oleophobic coating. This coating protects the nanocatalysts from the accumulation of adventitious carbon in air or solution environments. Because of this, heteroepitaxially deposited thin films of anatase nanocatalysts are an ideal platform for the study of anatase reactivity with atomic-scale precision, enabling the use of previously inaccessible techniques such as polarized infrared absorption spectroscopy.

Author Information

Corresponding Author

Melissa.Hines@cornell.edu, +1-607-255-3040

Notes

The authors declare no competing financial interest.

Acknowledgments

The authors would like to thank Amnon Ortoll Bloch for exploratory measurements. This work was supported by the National Science Foundation under Award CHE-1708025 and used the National Energy Research Scientific Computing Center, a DOE Office of Science User Facility supported by the Office of Science of the U.S. Department of Energy (DE-AC02-05CH11231) as well as the Cornell Center for Materials Research Shared Facilities supported through the NSF MRSEC program (DMR-1719875).

Supporting Information Available: The Supporting Information is available free of charge on the ACS Publications website.

X-ray diffraction analysis, XPS quantification, additional DFT simulations, representative structures used in DFT simulations.

References

[1] Selloni, A. Anatase Shows Its Reactive Side. *Nature Mater.* **2008**, *7*, 613-615.

[2] Yang, H. G.; Sun, C. H.; Qiao, S. Z.; Zou, J.; Liu, G.; Smith, S. C.; Cheng, H. M.; Lu, G. Q. Anatase TiO_2 Single Crystals With a Large Percentage of Reactive Facets. *Nature* **2008**, *453*, 638-641.

[3] Gordon, T. R.; Cargnello, M.; Paik, T.; Mangolini, F.; Weber, R. T.; Fornasiero, P.; Murray, C. B. Nonaqueous Synthesis of TiO_2 Nanocrystals Using TiF_4 to Engineer Morphology, Oxygen Vacancy Concentration, and Photocatalytic Activity. *J. Am. Chem. Soc.* **2012**, *134*, 6751-6761.

[4] Jun, Y.-W.; Casula, M. F.; Sim, J.-H.; Kim, S. Y.; Cheon, J.; Alivisatos, A. P. Surfactant-Assisted Elimination of a High Energy Facet as a Means of Controlling the Shapes of TiO_2 Nanocrystals. *J. Am. Chem. Soc.* **2003**, *125*, 15981-15985.

[5] Murakami, N.; Kurihara, Y.; Tsubota, T.; Ohno, T. Shape-Controlled Anatase Titanium(IV) Oxide Particles Prepared By Hydrothermal Treatment of Peroxo Titanic Acid in the Presence of Polyvinyl Alcohol. *J. Phys. Chem. C* **2009**, *113*, 3062-3069.

[6] Zhao, Y.; Ma, W.; Li, Y.; Ji, H.; Chen, C.; Zhu, H.; Zhao, J. The Surface-Structure Sensitivity of Dioxygen Activation in the Anatase-Photocatalyzed Oxidation Reaction. *Angew. Chem. Int. Ed.* **2012**, *51*, 3188-3192.

[7] Yella, A.; Lee, H.-W.; Tsao, H. N.; Yi, C.; Chandiran, A. K.; Nazeeruddin, M.; Diau, E. W.-G.; Yeh, C.-Y.; Zakeeruddin, S. M.; Grätzel, M. Porphyrin-Sensitized Solar Cells With Cobalt (II/III)-Based Redox Electrolyte Exceed 12 Percent Efficiency. *Science* **2011**, *334*, 629-634.

[8] O'Regan, B.; Grätzel, M. A Low-Cost, High-Efficiency Solar Cell Based on Dye-Sensitized Colloidal TiO_2 Films. *Nature* **1991**, *353*, 737-740.

[9] Hardin, B. E.; Snaith, H. J.; McGeehee, M. D. The Renaissance of Dye-Sensitized Solar Cells. *Nature Photonics* **2012**, *6*, 162-169.

[10] Inoue, T.; Fujishima, A.; Konishi, S.; Honda, K. Photoelectrocatalytic Reduction of Carbon Dioxide in Aqueous Suspensions of Semiconductor Powders. *Nature* **1979**, *277*, 637-638.

[11] Wang, R.; Hashimoto, K.; Fujishima, A.; Chikuni, M.; Kojima, E.; Kitamura, A.; Shimohigoshi, M.; Watanabe, T. Light-Induced Amphiphilic Surfaces. *Nature* **1997**, *388*, 431-432.

[12] Hoffmann, M. R.; Martin, S. T.; Choi, W.; Bahnemann, D. W. Environmental Applications of Semiconductor Photocatalysis. *Chem. Rev.* **1995**, *95*, 69-96.

[13] Zhang, L.; Cole, J. M. Anchoring Groups for Dye-Sensitized Solar Cells. *ACS Appl. Mater. Interfaces* **2015**, *7*, 3427-3455.

[14] Xu, M.; Gao, Y.; Moreno, E. M.; Kunst, M.; Muhler, M.; Wang, Y.; Idriss, H.; Wöll, C. Photocatalytic Activity of Bulk TiO_2 Anatase and Rutile Single Crystals Using Infrared Absorption Spectroscopy. *Phys. Rev. Lett.* **2011**, *106*, 138302.

[15] Vittadini, A.; Selloni, A.; Rotzinger, F. P.; Grätzel, M. Structure and Energetics of Water Adsorbed At TiO_2 Anatase (101) and (001) Surfaces. *Phys. Rev. Lett.* **1998**, *81*, 2954-2957.

[16] Herman, G. S.; Dohnálek, Z.; Ruzycki, N.; Diebold, U. Experimental Investigation of the Interaction of Water and Methanol With Anatase–TiO_2. *J. Phys. Chem. B* **2003**, *107*, 2788-2795.

[17] Tilocca, A.; Selloni, A. Methanol Adsorption and Reactivity on Clean and Hydroxylated Anatase (101) Surfaces. *J. Phys. Chem. B* **2004**, *108*, 19314-19319.

[18] Gong, X.-Q.; Selloni, A. Reactivity of Anatase TiO_2 Nanoparticles: The Role of the Minority (001) Surface. *J. Phys. Chem. B* **2005**, *109*, 19560-19562.

[19] Herman, G. S.; Sievers, M. R.; Gao, Y. Structure Determination of the Two-Domain (1 × 4) Anatase TiO_2 (001) Surface. *Phys. Rev. Lett.* **2000**, *84*, 3354-3357.

[20] Lazzeri, M.; Selloni, A. Stress-Driven Reconstruction of an Oxide Surface: The Anatase TiO_2(001)-(1×4) Surface. *Phys. Rev. Lett.* **2001**, *87*, 266105.

[21] Tanner, R. E.; Liang, Y.; Altman, E. I. Structure and Chemical Reactivity of Adsorbed Carboxylic Acids on Anatase TiO_2(001). *Surf. Sci.* **2002**, *506*, 251-271.

[22] Tanner, R. E.; Sasahara, A.; Liang, Y.; Altman, E. I.; Onishi, H. Formic Acid Adsorption on Anatase Tio_2(001)–(1×4) Thin Films Studied By NC-AFM and STM. *J. Phys. Chem. B* **2002**, *106*, 8211-8222.

[23] Ohsawa, T.; Lyubinetsky, I. V.; Henderson, M. A.; Chambers, S. A. Hole-Mediated Photodecomposition of Trimethyl Acetate on a TiO_2 Anatase Epitaxial Thin Film Surface. *J. Phys. Chem. C* **2008**, *112*, 20050-20056.

[24] Yuan, W.; Wang, Y.; Li, H.; Wu, H.; Zhang, Z.; Selloni, A.; Sun, C. Real-Time Observation of Reconstruction Dynamics on TiO_2(001) Surface Under Oxygen Via an Environmental Transmission Electron Microscope. *Nano Lett.* **2016**, *16*, 132-137.

[25] Skibinski, E. S.; Song, A.; DeBenedetti, W. J. I.; Ortoll-Bloch, A. G.; Hines, M. A. Solution Deposition of Self-Assembled Benzoate Monolayers on Rutile (110): Effect of π-π Interactions on Monolayer Structure. *J. Phys. Chem. C* **2016**, *120*, 11581-11589.

[26] Skibinski, E. S.; DeBenedetti, W. J. I.; Hines, M. A. Solution Deposition of Phenylphosphinic Acid Leads to Highly Ordered, Covalently Bound Monolayers on TiO_2(110) Without Annealing. *J. Phys. Chem. C* **2017**, *121*, 14213-14221.

[27] Kohn, W.; Sham, L. J. Self-Consistent Equations Including Exchange and Correlation Effects. *Phys. Rev.* **1965**, *140*, A1133-A1138.

[28] Perdew, J. P.; Burke, K.; Ernzerhof, M. Generalized Gradient Approximation Made Simple. *Phys. Rev. Lett.* **1996**, *77*, 3865-3868.

[29] Grimme, S.; Antony, J.; Ehrlich, S.; Krieg, H. A Consistent and Accurate *Ab Initio* Parameterization of Density Functional Dispersion Correction (DFT-D) for the 94 Elements H-Pu. *J. Chem. Phys.* **2010**, *132*, 154104.

[30] Kresse, G.; Hafner, J. *Ab Initio* Molecular Dynamics for Liquid Metals. *Phys. Rev. B* **1993**, *47*, 558-561.

[31] Kresse, G.; Furthmüller, J. Efficient Iterative Schemes for *Ab Initio* Total-Energy Calculations Using a Plane-Wave Basis Set. *Phys. Rev. B* **1996**, *54*, 11169-11186.

[32] Blöchl, P. E. Projector Augmented-Wave Method. *Phys. Rev. B* **1994**, *50*, 17953-17979.

[33] Tersoff, J.; Hamann, D. R. Theory of the Scanning Tunneling Microscope. *Phys. Rev. B* **1985**, *31*, 805-813.

[34] Sun, C.; Selloni, A.; Du, A.; Smith, S. C. Interaction of Water With the Fluorine-Covered Anatase TiO_2 (001) Surface. *J. Phys. Chem. C* **2011**, *115*, 17092-17096.

[35] Yamamoto, S.; Bluhm, H.; Andersson, K.; Ketteler, G.; Ogasawara, H.; Salmeron, M.; Nilsson, A. *In Situ* X-Ray Photoelectron Spectroscopy Studies of Water on Metals and Oxides At Ambient Conditions. *J. Phys.: Condens. Matter* **2008**, *20*, 184025.

[36] Blomquist, J.; Walle, L. E.; Uvdal, P.; Borg, A.; Sandell, A. Water Dissociation on Single Crystalline Anatase TiO_2(001) Studied By Photoelectron Spectroscopy. *J. Phys. Chem. C* **2008**, *112*, 16616-16621.

[37] Landis, E. C.; Jensen, S. C.; Phillips, K. R.; Friend, C. M. Photostability and Thermal Decomposition of Benzoic Acid on TiO_2. *J. Phys. Chem. C* **2012**, *116*, 21508-21513.

[38] Song, A.; Skibinski, E. S.; DeBenedetti, W. J. I.; Ortoll-Bloch, A. G.; Hines, M. A. Nanoscale Solvation Leads to Spontaneous Formation of a Bicarbonate Monolayer on Rutile (110) Under Ambient Conditions: Implications for CO_2 Photoreduction. *J. Phys. Chem. C* **2016**, *120*, 9326-9333.

[39] DeBenedetti, W. J. I.; Skibinski, E. S.; Hinckley, J. A.; Nedessa, S. B.; Hines, M. A. Cartesian Decomposition of Infrared Spectra Reveals the Structure of Solution-Deposited, Self-Assembled Benzoate and Alkanoate Monolayers on Rutile (110). *J. Phys. Chem. C* **2016**, *120*, 24866-24876.

[40] Gong, X.-Q.; Selloni, A.; Vittadini, A. Density Functional Theory Study of Formic Acid Adsorption on Anatase TiO_2(001): Geometries, Energetics, and Effects of Coverage, Hydration, and Reconstruction. *J. Phys. Chem. B* **2006**, *110*, 2804-2811.

[41] Barrow, H.; Brown, D. A.; Alcock, N. W.; Clase, H. J.; Wallbridge, M. G. H. Reactions of Titanium Tetrachloride With Carboxylic Acids. Crystal and Molecular Structure of the Dinuclear Titanium Oxo Compound [$\{TiCl_2(O_2CBu^t)(Bu^tCO_2H)\}_2O$]. *J. Chem. Soc. Dalton Trans.* **1994**, 195-199.

[42] Selçuk, S.; Selloni, A. Surface Structure and Reactivity of Anatase TiO_2 Crystals With Dominant {001} Faces. *J. Phys. Chem. C* **2013**, *117*, 6358-6362.

TOC Graphic